

What Electronic Image Noise Signatures Can Tell Us About Image Linearity and Camera Encoding

Ricardo R. Figueroa, PhD

Rochester Institute of Technology

**Written for presentation at the
SMPTE 2023 Media and Technology Summit**

Abstract. *Electronic image noise is often categorized as an artifact of image capture which typically requires correction. There are several sources of electronic image noise that contribute to the overall total noise in an image. Some of the noise from specific sources, known as systematic noise, can be corrected for in-camera, but noise due to certain sources, like photon noise, persists after capture and increases with exposure. We study this relationship between exposure and noise and discover that this relationship reveals information about the linearity, or non-linearity of the image encoding. Non-linear encoding of images through an Opto-Electronic Transfer Function (OETF) is a typical image processing step that allows for perceptually efficient use of encoding bit depth, and the accurate measurement or estimation of the OETF becomes necessary for proper processing of images through motion picture post-production workflows like the Academy Color Encoding Specification (ACES), helping minimize non-creative manual adjustments, or when combining natural images with radiometrically linear Computer Generated Imagery (CGI). Although there are well known standard OETFs implemented in typical video camera workflows, motion picture camera workflows have introduced new standard OETFs as well as custom and/or proprietary OETFs. Existing methods to measure or estimate this function rely on the use of test charts, restrictive exposure and/or lighting conditions, or assume a simplistic model of the function's shape. All these methods become problematic and tough to fit into motion picture production and post-production workflows where the use of test charts and varying camera or scene setups becomes impractical. We propose a method based on the relationship between exposure and noise mentioned above and*

The authors are solely responsible for the content of this technical presentation. The technical presentation does not necessarily reflect the official position of the Society of Motion Picture and Television Engineers (SMPTE), and its printing and distribution does not constitute an endorsement of views which may be expressed. This technical presentation is subject to a formal peer-review process by the SMPTE Board of Editors, upon completion of the conference. Citation of this work should state that it is a SMPTE meeting paper. EXAMPLE: Author's Last Name, Initials. 2022. Title of Presentation, Meeting name and location.: SMPTE. For information about securing permission to reprint or reproduce a technical presentation, please contact SMPTE at jwelch@smpte.org or 914-761-1100 (445 Hamilton Ave., White Plains, NY 10601).

demonstrate how this relationship reveals information that can be used in an inference framework to estimate the OETF, and in turn, linearize images for accurate processing, when necessary, without the need for charts or specific image capture conditions. In addition, we present the limitations of our method, for example, where extensive and/or adaptive noise correction can prevent our method from an accurate estimation of the OETF.

Keywords. *Radiometric Calibration, Opto-Electronic Transfer Function (OETF), Camera Response Function (CRF)*

The authors are solely responsible for the content of this technical presentation. The technical presentation does not necessarily reflect the official position of the Society of Motion Picture and Television Engineers (SMPTE), and its printing and distribution does not constitute an endorsement of views which may be expressed. This technical presentation is subject to a formal peer-review process by the SMPTE Board of Editors, upon completion of the conference. Citation of this work should state that it is a SMPTE meeting paper. EXAMPLE: Author's Last Name, Initials. 2022. Title of Presentation, Meeting name and location.: SMPTE. For information about securing permission to reprint or reproduce a technical presentation, please contact SMPTE at jwelch@smpte.org or 914-761-1100 (445 Hamilton Ave., White Plains, NY 10601).

Introduction

Digital processes today generate large amounts of data. These processes exist in many applications and in most cases, the generated data exists by itself without any information or details about the process that created it. It is of interest to use computers to analyze the data, learn information about the process, and be able to predict future data from an estimation of the process that generated that data.

One of such processes is the capture of images by an electronic camera. Different cameras have different ways of encoding the light being captured from a scene. This encoding converts the light falling onto the imaging sensor into digital pixel code values that are then manipulated in post-production. One of the most important steps in this encoding is the Opto-Electronic Transfer Function (OETF) which allows the camera to have a more efficient encoding and to encode the light from the scene in a way that mimics the human visual system. Another important typical step following the implementation of the OETF is a color encoding transform that ensures subsequent appropriate display color reproduction. Although the main objective of the OETF is similar for all cameras, different camera manufacturers implement different types of functions due to different existing standards, advancements in camera technology, proprietary advantages, and image sensor characteristics to name a few reasons.

To reduce time-consuming technical adjustments in post-production, it is desired to implement methods that estimate camera specific characteristics that created the images, like the OETF, without the need for analysis procedures that are not viable or practical in production or post-production environments. Typical television or motion picture productions involve different image manipulation workflows that are very challenging to integrate. Many of these productions can use various capture mediums in the production. Add to this the fact that during post-production, images from different sources can arrive at a facility in several different formats, color encodings and sometimes without helpful metadata. An example encoding system to solve some of these issues is the Academy Color Encoding System (ACES) and its Input Device Transform (IDT) which aims at characterizing every possible input so it can be integrated into the ACES workflow. The OETF is a key camera characteristic that needs to be known for the accurate calculation and/or implementation of an IDT, since it relates camera code values to linear scene radiometry.

Previous Work

Aside from measuring the OETF through direct photography of a variable reflectance or transmittance test chart, some of the most popular methods for estimating it involve taking multiple registered images of a static scene while varying the camera exposure^{1,2}. Work has also been done by Grossberg and Nayar³ to relax this dependency on multiple spatially registered images by using histograms of images at different exposures. Manders, C. et al.⁴ estimate the response by capturing registered images of a static scene illuminated by different combinations of light sources and locking the exposure instead of varying it. Similar work was presented by Kim et al.⁵ where the estimation is done based on a video sequence with varying exposure. All these methods require significant effort to obtain a series of registered, static scene or exposure dependent images. Other approaches, like Farid⁶, assume that the response function has the form of a gamma curve to estimate it from one single image by exploiting the

fact that the non-linearity introduced by the gamma correction also introduces higher-order correlations in the frequency domain that can be detected with tools from polyspectral analysis. However, many cameras in use today in the motion picture industry have OETFs that differ significantly from a gamma curve, especially higher end motion picture cameras where their design deviates from the typical video imaging paradigm. Lin et al.⁷ estimate the response by looking at the edge color distributions in a single image.

Other work has focused on using multiple images, especially photo collections. Diaz and Sturm⁸ use a set of images from an internet collection to recover the camera's geometric calibration and a 3D scene model, which in turn are used as input to determine the camera radiometric response function. The requirement to obtain the scene 3D model would be an undesired workflow step for motion picture post-production workflows focused on image integration and color correction. Shafique et al.⁹ introduce a method that uses differently illuminated images and estimates the response function by assuming that the properties of materials in a scene should remain constant and use cross-ratios of image values in the different color channels to compute the response function. They also model the response function as a gamma curve. This again excludes the modeling of cameras that have OETFs that differ from a gamma curve and their algorithm was only verified by synthetic experiments. Kuthirummal et al.¹⁰ found priors for statistics in large photo collections and use them to estimate the response function of generic camera models if all instances of a camera model have the same properties and that many images are available for that specific camera. A major disadvantage of their method is that it doesn't allow modeling of cameras with interchangeable lenses. This is also an impractical approach for the motion picture industry. Lastly, our previous work¹¹, expands on the work of Lin et al. by extending their framework to the use of multiple images and estimating the posterior probability distribution, and serves as the basis for the methodology presented in this paper.

Many of the existing methods described above suffer from the following general practical limitations in their application to the motion picture industry. They are restrictive in the position or movement of the capture device, they are restrictive in the exposure required for the camera sensor, and they wrongly assume a simplistic mathematical formulation of the OETF, or they require co-capture of images plus additional scene information. Our proposed approach explained in the following sections again looks avoid these limitations and provide a solution based on typical motion picture images.

Radiometric Calibration Background

The radiometric camera response function f relates captured scene radiance I , or proportional image irradiance, to its measured intensity M in the image, represented by the pixel code value:

$$M = f(I) \quad (1)$$

Typically, radiometric calibration methods solve for the inverse response function $g = f^{-1}$, which is invertible since the sensor output increases monotonically with respect to I . Popular previous works relying on multiple exposures compute the inverse response function based on the relationship:

$$g(m_A) = kg(m_B) \quad (2)$$

where m_A and m_B represent image intensities in images A and B respectively for corresponding points and k denotes the exposure ratio between the two images. Requirements like precise registration of images or known exposure ratios have been worked around with the use of histogram equalization and the use of iterative methods, referenced in the previous section, to solve for k and g .

One important obstacle in computing the camera radiometric response function from Equation 2 is the exponential ambiguity. From Equation 2, if g and k are solutions for a specific image set, then g^u and k^u could also be solutions. To deal with this ambiguity, these prior methods require a good initial estimate of the exposure ratio if unknown, and assumptions on the structure of the radiometric function model as presented by Grossberg and Nayar¹². Their results present a relationship between image intensity $M = f(I)$ and image irradiance I that can be expressed as a linear combination of an average camera response function h_0 and principal components h_n :

$$f(I) = h_0(I) + \sum_{n=1}^N w_n h_n(I) \quad (3)$$

This principal component analysis (PCA) approach produces the mathematical model of the OETF.

Bayesian Inference Framework

Probability based estimation methods have been used for many years and in many applications¹⁴. Two popular solution approaches for these estimation methods are maximum likelihood (ML) and maximum a posteriori (MAP)¹⁵. In the case of ML, the result produces the choice most likely to have generated the available data. MAP produces the choice that is most likely, given the available data. An important difference is that MAP estimation applies Bayes' Rule, shown in equation 4, so that the estimate can consider prior parameter knowledge in the form of a prior probability distribution, $p(g)$, while evaluating the likelihood of the data, $p(\Omega | g)$, generated by those parameters. MAP can be considered an improvement over ML, but both ML and MAP give only single point best estimates and not a distribution of the parameters in question, although a benefit is that these methods typically compute this single best estimate in a fast and efficient manner.

$$p(g|\Omega) = \frac{p(\Omega|g)p(g)}{p(\Omega)} = \frac{p(\Omega|g)p(g)}{\int_g p(\Omega|g)p(g)dg} \quad (4)$$

Prior Probability Distribution

The prior model was created from the Database of Response Functions (DoRF) compiled by Grossberg and Nayar¹². This database contains 201 inverse response functions from a variety of digital cameras and films up to the year 2003. The prior probability distribution based on this database, $p(g)$, describes prior knowledge about the mathematical description and space of OETFs and is modeled as a Gaussian Mixture Model (GMM), with means and covariances μ_i, Σ_i for each mixture component i and mixture proportion α_i . In our implementation the prior was precomputed using the Expectation Maximization (EM) algorithm.

$$p(g) = \sum_{i=1}^K \alpha_i N(g; \mu_i, \Sigma_i) \quad (5)$$

Bayesian MAP Solution

After modeling the prior and the likelihood functions, the problem can be formulated with a MAP solution approach as described in equations 7 and 8. The optimal response function for a data set Ω , is then described as:

$$g = \arg \max p(g | \Omega) = \arg \max p(\Omega | g) p(g) \quad (7)$$

Or taking the log of equation 7, g can also be written as:

$$g = \arg \min \lambda D(g; \Omega) - \log p(g) \quad (8)$$

This again represents a single point best estimate of the inverse OETF, g .

Posterior Probability Distribution

As mentioned in the previous section, a benefit of ML and MAP is that these methods compute a single best estimate that can be easily and efficiently calculated, but this comes at the cost of throwing away information included in the posterior probability distribution, $p(g | \Omega)$ in equation 4, due to the cost of computing the integral in the denominator over a high dimensional space. To do this, we realize that the integral in the denominator in equation 4 is an expected value calculation that can be approximated, allowing us to estimate the posterior distribution of g rather than just a single best estimate. This expectation is shown in equation 9 for the general continuous case.

$$E[f(z)] = \int f(z) p(z) dz \quad (9)$$

Here z is the random variable, and $p(z)$ is the probability distribution over possible values of z . In our case we are interested in calculating the expected value of $f(z) = p(\Omega | g)$, which is the probability of the data given g , the likelihood. This expectation is taken over the whole distribution of possible values of g , $p(g)$, the prior.

Markov Chain Monte Carlo (MCMC)

The problem in calculating the expected value in equation 9 arises from the fact that computing the integral in the denominator of equation 4 is in many cases an intractable problem¹³. Conceptually, this integral sums up $p(\Omega | g) p(g)$ over all values of g , in a highly dimensional space. Since we are interested in approximating this integral because of the high dimensionality, another way to think about the calculation is to sample N points $z(1), z(2), z(3) \dots z(N)$ from the distribution $p(\Omega | g)$ at random with respect to the prior probability density function $p(g)$, giving us the expected value in the following form.

$$E_{p(z)} [f(z)] = \lim_{N \rightarrow \infty} \frac{1}{N} \sum_{t=1}^N f(z^{(t)}) \quad (10)$$

By thinking of the problem in this way, we can implement a Markov chain Monte Carlo (MCMC) sampling algorithm, like the Metropolis-Hastings algorithm¹³, to approximate the posterior probability distribution for g given a set of image pixel data Ω , and obtain an expected value from that approximation, as equation 10 shows.

Image Noise Background

The total noise in the image data captured by an imaging sensor is a combination of several independent sources of noise. These include photon noise, read noise, which includes a fixed pattern noise component, thermal noise, pixel response non-uniformity noise and the quantization error. Equation 11 shows how different independent noise sources, $N_1, N_2, N_3 \dots N_n$ are added in quadrature to contribute to the total noise N_t .

$$N_t = \sqrt{N_1^2 + N_2^2 + N_3^2 + \dots + N_n^2} \quad (11)$$

Photon noise is the noise associated with the fluctuations around the average flux of photons arriving at an imaging sensor. These fluctuations are governed by Poisson statistics, and they are equal to the square root of the average flux, or number of photons, counted by the imaging sensor. Equation 12 shows this relationship, where N_{ph} represents the photon noise and P represents the photon count.

$$N_{ph} = \sqrt{P} \quad (12)$$

Read noise, N_R , is associated with the fluctuations introduced by the electronic components present in the readout, gain and digitization circuitry of the sensor at each pixel. The digitized signal is ideally directly proportional to the photon count that arrived at each pixel. But in real camera systems, the read noise introduces a deviation in the raw measured code value. As an example, the read noise can be isolated and measured by capturing a black frame. This implies taking a frame, or a few frames, with a lens cap on, to avoid light hitting the sensor, at the highest shutter speed, or shortest integration time, possible. Once this black frame is captured, the read noise can be calculated as the standard deviation of that frame, since all variation is solely due to the electronics and not to any arriving photons. A component of the read noise is the fixed pattern noise, and it can be isolated by taking the average of J black frames, typically ten or more. This averaging has the effect of removing the variable component of the noise, reducing it by a factor of \sqrt{J} relative to the fixed pattern component, and leave only a fixed pattern noise template, that can then be subtracted by the camera processing.

A third noise component is thermal noise. Thermal noise is due to the thermal agitation of electrons in a sensor pixel, and they are indistinguishable from electrons generated by an exposure. The thermal noise tends to rise with exposure time, but this is not a concern for motion imaging applications as the exposure time is set consistent each time and it is restricted by the chosen frame rate of the motion imaging camera.

Pixel response non-uniformity (PRNU) is related to the difference from pixel to pixel in the efficiency to capture and count arriving photons. PRNU grows proportionally with the exposure level, and it is the most dominant noise component at high exposure levels if not accounted for in the camera processing. The relationship between PRNU and raw code values is given by equation 13, where N_{PRNU} represents the PRNU noise, v represents the variation in the response of each pixel and S_{AVG} represents the average raw code value.

$$N_{PRNU} = v \cdot S_{AVG} \quad (13)$$

The last noise component is the quantization error. This noise is due to the rounding off in the conversion from an analog voltage signal into a digitized raw code value. The contribution of this error to the noise is considered negligible in modern electronic motion imaging cameras.

In modern camera systems, some of these contributors to noise will be minimized by in-camera processing. As described above, the fixed component of the read noise can be eliminated by averaging several black frames. The PRNU can also be eliminated by a process called flat field correction since it is a fixed property of the imaging sensor that does not change from image to image. The process involves again taking J number of images of an evenly illuminated featureless surface. Since PRNU is most dominant at higher exposures, and the variable photon

noise will also be an important contributor at those exposure levels, taking the average of J flat field images will reduce the variable photon noise by a factor of \sqrt{J} relative to the PRNU. Now, PRNU is a variation on each pixel's response to light. The average flat field image represents a map of that variation and can then be used to divide the captured image pixel code values by the flat field image pixel code values, removing the variation in pixel-to-pixel response. This will also have the effect of dividing the pixel code values by the average illumination level of the flat field image L_{AVG} , so it will need to be restored in the correction. Equation 14 shows how both the fixed pattern correction and PRNU correction are implemented where I_C is the corrected image, I_U is the uncorrected image, FP_T is the fixed pattern noise template and $PRNU_T$ is the flat field PRNU template. Applying the correction in this way also takes care of removing any camera specific code value offset applied to images, as the fixed pattern template would include the offset.

$$I_C = \frac{L_{AVG} \cdot (I_U - FP_T)}{(PRNU_T - FP_T)} \quad (14)$$

Although these noise contributions from fixed pattern noise and PRNU can be minimized or eliminated in modern camera systems, contributions from the variable component of the read noise and from photon noise are going to be present in every image. This allows for the introduction of a noise image signature that can be used in our Bayesian framework to estimate the inverse OETF.

Noise Image Signatures

As shown in the previous section, many sources of noise combine when capturing an electronic image, and some of these sources can be eliminated or discounted. The two most important sources of noise considered in typical exposures are read noise, N_R , and photon noise, N_{Ph} , and together they determine the image quality and signal to noise ratio at a given exposure. The two can be combined in quadrature to determine the total noise, N_T , as presented in equation 15.

$$N_T^2 = N_R^2 + N_{Ph}^2 \quad (15)$$

Photon noise is dictated by Poisson statistics as shown in equation 12, where the photon noise is the square root of the average photon count. Image data is accessible in the form of raw code values instead of photon counts and there exists a proportionality constant that relates this photon count and the raw code value. This is known as the gain, and it is represented with the variable g_c . This allows equation 12 to be rewritten in terms of code values (CV). With g_c photons/CV, the noise and the photon count are represented in code values as $N_{PhCV} = N_{Ph}/g_c$ and $S_{CV} = P/g_c$, and equation 12 can be rewritten in the following form:

$$N_{PhCV} = \sqrt{S_{CV}} \quad (16)$$

In addition, g_c is inversely proportional to the camera ISO setting, $g_c = ISO_N/ISO$, where ISO represents the camera ISO setting and ISO_N is a constant that represents the native ISO of the camera, which is reported by the camera manufacturer.

This results in the following relationship between the photon noise code value, the signal code value, and the gain.

$$N_{PhCV}^2 = \left(\frac{N_{Ph}}{g_c} \right)^2 = \frac{N_{Ph}^2}{g_c^2} = \frac{P}{g_c^2} = \frac{S_{CV} \cdot g_c}{g_c^2} = \frac{S_{CV}}{g_c} \quad (17)$$

Now equation 15 can be expressed in the following form where the total noise, read noise and photon noise are obtained by measuring the noise and signal in pixel code values. This allows the measurement of the noise at a variety of exposure levels, plotting the square of the noise versus the average code value and fitting it to a straight line, where the inverse of the slope is the gain controlled by the camera ISO setting, and the y-axis intercept is the read noise squared. This is illustrated in figure 1 for a linear image with no OETF applied.

$$N_T^2 = N_R^2 + \frac{S_{CV}}{g_c} \quad (18)$$

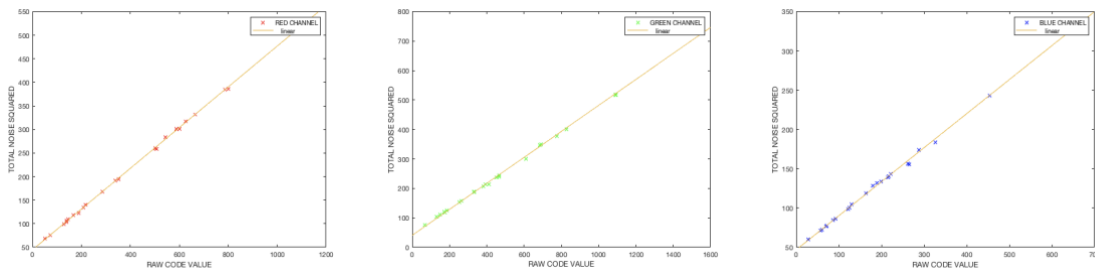


Figure 1. Linear relationship between the square of the total noise versus the measured pixel code value for channels R, G, and B.

Figure 2 shows the effect of applying an OETF to the image. This non-linearity of the total noise squared vs. average code values is the noise image signature used to estimate the OETF, and processing the image through the inverse OETF restores the linear relationship.

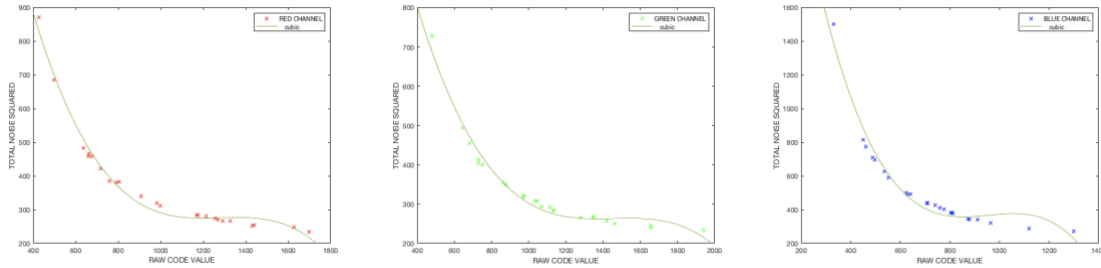


Figure 2. Non-linear relationship between the square of the total noise and the measured pixel code value for channels R, G, and B. This is introduced by applying an OETF.

Pearson Correlation Coefficient

Examining equation 18, it is necessary to define a metric that indicates the level of linearity between the squared noise measurements versus code values. The Pearson correlation coefficient can be used to measure this linearity between the squared noise variable and the code value variable. In addition, the distance metric known as Pearson distance is also used. The Pearson distance will have minimum value of 0, for a total positive correlation and a maximum value of 2 for a total negative correlation. This distance can then be incorporated into the likelihood probability exponential distribution as described earlier. Equations 19 and 20 show the Pearson correlation coefficient for random variables X and Y , and corresponding mean and standard deviations, μ and σ , and the Pearson distance calculation.

$$\rho_{X,Y} = \frac{\text{cov}(X, Y)}{\sigma_X \cdot \sigma_Y} = \frac{E[(X - \mu_X) \cdot (Y - \mu_Y)]}{\sigma_X \cdot \sigma_Y} \quad (19)$$

$$d = 1 - \rho_{X,Y} \quad (20)$$

Figure 3 shows sample Pearson correlation coefficients for various examples of a scatter diagram between random variables X and Y .

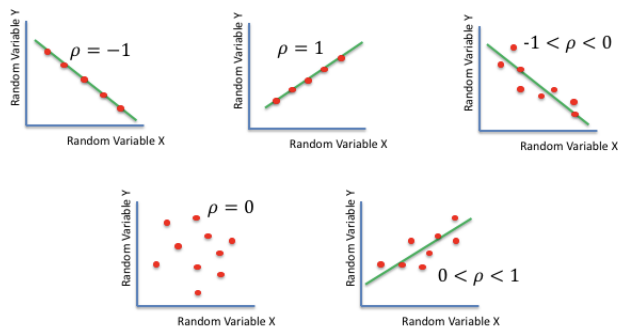


Figure 3. Sample Pearson correlation coefficient values for different random variable relationships.

Image Noise Area Detection

Figures 1 and 2 show the total squared noise versus code value relationship utilizing images of a color checker, or similar chart, to ensure smooth nontextured image surfaces appropriate for noise measurements. This is a practical process to follow in a laboratory environment to validate the methodology, but very impractical for typical production workflows. This research aims to compute this for any non-textured image areas where the measurement can be done reliably. The task of detecting these areas in typical images is carried out in two general steps. First, an edge detection algorithm is used. This step ensures that true edges and textured image areas are detected. Second, the edge map created in the edge detection stage is used to exclude those areas from where noise measurements can be done. Various patch regions sizes were tested and negligible OETF estimation result differences were found for patch sizes 25×25 or larger, although the algorithm performance was impacted by patch sizes above 50×50 . The patch size was empirically selected to 30×30 pixels for most experiments. The total number of patches was also empirically selected to be between 500-1000 patches per image. Figure 4 shows an example edge map and subsequent patches selected for noise analysis. Figures 5 and 6 show the non-linear image noise signatures for the red, green, and blue channels, for an ARRI camera, and the subsequent noise signatures after OETF linearization.

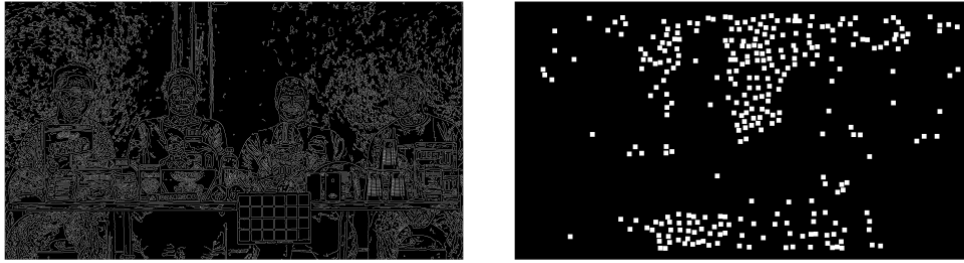


Figure 4. Example edge detected image and accompanying noise patch detection avoiding textured image areas identified by the edge detection algorithm.

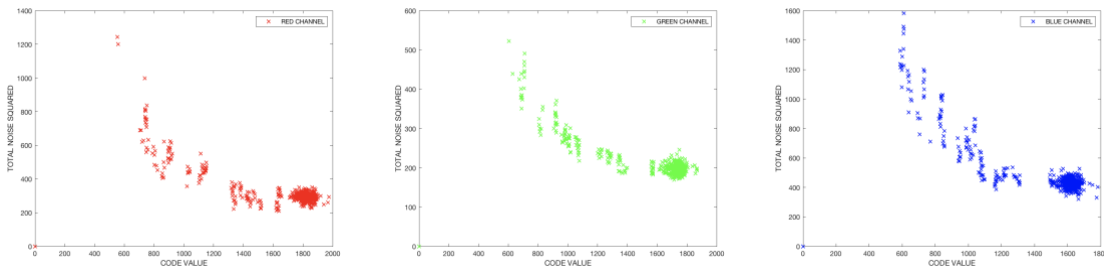


Figure 5. Non-linear relationship between total squared noise and the measured pixel value for R, G, and B channels, for an ARRI camera image.

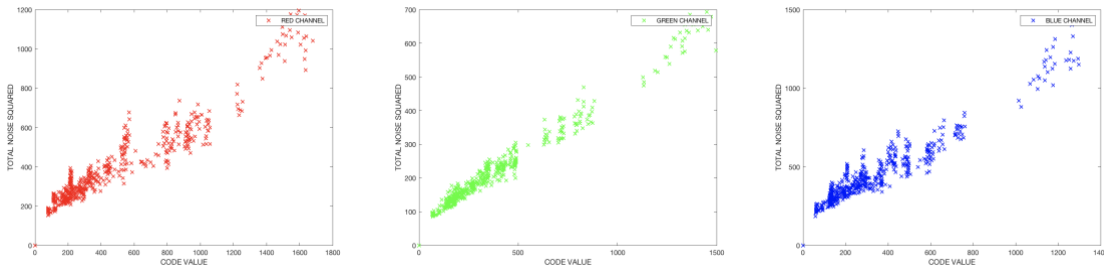


Figure 6. Non-linear relationship correction through inverse OETF, between Total squared noise and the measured pixel value for R, G, and B channels, for ARRI camera image.

OETF Estimation Results

Our Bayesian inference method was implemented to estimate the posterior distribution of the OETF. Figure 7 shows the OETF (inverse of g) expected value, compared with the actual measured OETF for an example camera. RMS errors obtained were .017, .020, .020 for the red, green, and blue channels respectively, showing comparable and modest improvement over our previous approach¹¹.

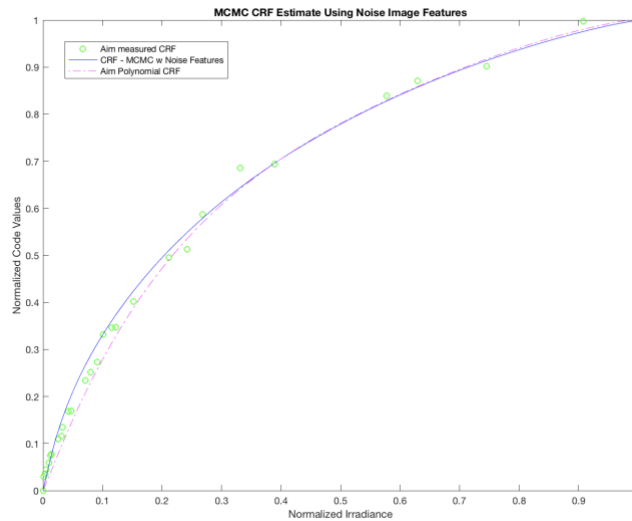


Figure 7. OETF estimation comparison with posterior probability distribution sampling and OETF expected value calculation, including noise image features.

Methodology Limitations

When considering our methodology, aggressive spatial image processing can affect the distance calculation in equation 20. As well, aggressive noise reduction can also adversely impact the ability to measure the photon/read noise at different non-textured areas of the image and consequently affect the accurate estimation of the OETF. In addition, very low dynamic range images, e.g., very dark, very bright images, or extremely low contrast images, can present a challenge in obtaining enough data for the calculation of the Pearson coefficient. The linearity of the data presented on figure 1 is best represented and visualized with code values across a large dynamic range of the camera system, versus a reduced number of measurements grouped together in any single area of the camera dynamic range, which can affect the accurate calculation of the Pearson correlation coefficient and Pearson distance. Lastly, highly textured image content can present a challenge in the identification of enough nontextured image areas to compute the total noise at different parts of the dynamic range of the camera.

Conclusions

The methodology described in this work is a viable solution for estimating an electronic camera OETF from captured digital images. This again is an important computation when the OETF is not known from metadata or from a direct measurement. In many cases, only captured digital images, and not the camera or accompanying metadata, are available when incorporating said images into a motion picture post-production workflow. An OETF will typically represent a non-linear relationship between the scene radiometry and the measured pixel code value for benefits including encoding efficiency and perceptual accuracy. Understanding this non-linearity is also important to ensure the proper calculation or implementation of color space transformations like the ACES IDT. The calculation of the IDT assumes a linear relationship between the exposures captured by the camera system and the measured pixel code values, and any non-linearity still present in the image pixel code values at the time of calculating or implementing an IDT, can result in color errors that can prevent efficient post-production workflows.

References

1. T. Mitsunaga and S.K. Nayar. "Radiometric Self Calibration". In *Computer Vision and Pattern Recognition*, 1999. IEEE Computer Society Conference, volume 1, pages 2 vol. (xxiii+637+663), 1999.
2. Paul E. Debevec and Jitendra Malik. "Recovering High Dynamic Range Radiance Maps from Photographs". In *Proceedings of the 24th annual conference on Computer Graphics and Interactive Techniques, SIGGRAPH '97*, pages 369–378, New York, NY, USA, 1997. ACM Press/Addison-Wesley Publishing Co.
3. M.D. Grossberg and S.K. Nayar. "Determining the Camera Response from Images: What Is Knowable?" *Pattern Analysis and Machine Intelligence*, IEEE Transactions, 25(11):1455 – 1467, Nov. 2003.
4. C. Manders, C. Aimone, and S. Mann. "Camera Response Function Recovery from Different Illuminations of Identical Subject Matter". In *Image Processing, 2004. ICIP '04. 2004 International Conference*, volume 5, pages 2965 – 2968.
5. Seon Joo Kim, J.-M. Frahm, and M. Pollefeys. "Joint Feature Tracking and Radiometric Calibration from Auto-Exposure Video". In *Computer Vision, 2007. ICCV 2007. IEEE 11th International Conference on*, pages 1 –8, Oct. 2007.
6. H. Farid. "Blind Inverse Gamma Correction". *Image Processing*, IEEE Transactions, 10(10):1428 –1433, Oct. 2001.
7. S. Lin, Jinwei Gu, S. Yamazaki, and Heung-Yeung Shum. "Radiometric Calibration

- from a Single Image”. In *Computer Vision and Pattern Recognition*, 2004. CVPR 2004. *Proceedings of the 2004 IEEE Computer Society Conference*, volume 2, pages II–938 – II–945 Vol.2, July 2004.
8. M. Diaz and P. Sturm. “Radiometric Calibration Using Photo Collections”. In *Computational Photography (ICCP)*, 2011 IEEE International Conference, pages 1 –8, April 2011.
 9. K. Shafique and M. Shah. “Estimation of the Radiometric Response Function of a Color Camera from Differently Illuminated Images”. In *Image Processing, 2004. ICIP '04. 2004 International Conference*, volume 4, pages 2339–2342 Vol. 4, Oct. 2004.
 10. Sujit Kuthirummal, Aseem Agarwala, Dan B Goldman, and Shree K Nayar. “Priors for Large Photo Collections and What They Reveal About Cameras”. In *Computer Vision–ECCV 2008*, pages 74–87. Springer, 2008.
 11. Ricardo R. Figueroa and Rui Li. “Bayesian methods for radiometric calibration in motion picture encoding workflows”. *SMPTE Motion Imaging Journal*, 128(7):25–30, Aug 2019.
 12. M.D. Grossberg and S.K. Nayar. “Modeling the Space of Camera Response Functions”. *Pattern Analysis and Machine Intelligence*, IEEE Transactions, 26(10):1272 –1282, Oct. 2004.
 13. Christophe Andrieu, Nando De Freitas, Arnaud Doucet, and Michael I Jordan. “An introduction to MCMC for machine learning”. *Machine Learning*, 50(1-2):5–43, 2003.
 14. Modeling eye movement patterns to characterize perceptual skill in image-based diagnostic reasoning processes Li R., Shi P., Pelz J., Alm C.O., Haake A.R. (2016) *Computer Vision and Image Understanding*, 151, pp. 138-152.
 15. Christopher M. Bishop. 2006. *Pattern Recognition and Machine Learning* (Information Science and Statistics). Springer-Verlag, Berlin, Heidelberg.
 16. Ricardo R. Figueroa and Jinwei Gu. “Camera Radiometric Calibration from Motion Images”. In Annual Technical Conference Exhibition, SMPTE 2013, pages 1–10, Oct. 2013.